Heavy neutrinos at the FCC-hh in the $U(1)_{B-L}$ model

Wei Liu,[1,2,*] Suchita Kulkarni,[3,†] and Frank F. Deppisch[2,‡]

[1]Department of Applied Physics, Nanjing University of Science and Technology, Nanjing 210094, China
[2]University College London, Gower Street, London WC1E 6BT, United Kingdom
[3]Institute of Physics, NAWI Graz, University of Graz, Universitätsplatz 5, A-8010 Graz, Austria

(Received 6 March 2022; accepted 21 April 2022; published 27 May 2022)

We investigate the potential of the 100 TeV future circular collider (FCC-hh) to probe heavy neutrinos. We concentrate in particular on heavy neutrino production via a $U(1)_{B-L}$ Z' gauge boson and contrast the resulting limits with that mediated by Standard Model weak currents. We consider heavy neutrino decays to semileptonic as well as fully leptonic final states, particularly with muon flavor, and we show the importance of considering searches both in prompt and displaced decays of the heavy neutrinos. For prompt final states, semileptonic modes are more promising due to smaller background and larger yields, and TeV-scale heavy neutrinos with active-sterile mixing compatible with light neutrino mass generation in a seesaw scenario can be probed for a 5 TeV Z' and gauge coupling as low as $g_{B-L} = 10^{-2}$. Displaced vertex searches can extend this range to heavy neutrino masses as low as 10 GeV.

DOI: 10.1103/PhysRevD.105.095043

I. INTRODUCTION

The observation of small neutrino masses, which have no explanation within the Standard Model (SM) of particle physics, points towards new physics. Among possible scenarios that can explain neutrino masses, the $U(1)_{B-L}$ gauge model is one of the simplest anomaly free constructions [1,2]. It incorporates three right-handed (RH) neutrinos N_i, which acquire Majorana masses upon the spontaneous breaking of the $U(1)_{B-L}$ gauge symmetry. In turn, this induces light active neutrino masses via the seesaw mechanism. As opposed to the minimal seesaw scenario, the RH neutrinos are not completely sterile under the model's gauge symmetry. Instead, they are charged under $U(1)_{B-L}$ and they couple to the associated heavy gauge boson Z' and $B-L$ charged Higgs χ present in the model. This opens up a rich phenomenology as it not only provides the SM charged and neutral current portals for heavy neutrino production but also production via the Z' and χ.

The $B-L$ production mechanisms are not suppressed by the active-sterile mixing that is generically expected to be very small, $|V_{lN}| \sim \sqrt{m_\nu/m_N} \lesssim 10^{-6} \times (100\ \text{GeV}/m_N)$, to accommodate the observed light neutrino masses $m_\nu \lesssim 0.1$ eV. For such a small active-sterile mixing, the heavy neutrinos, which can only decay through such suppressed channels, are long-lived with a proper decay length $L_N^0 \sim 2.5\,\text{cm} \times (10^{-6}/|V_{lN}|)^2 (100\,\text{GeV}/m_N)^5$ for $m_N \lesssim 100$ GeV. This naturally leads to displaced vertex signatures at colliders for heavy neutrino masses $m_N \approx 100$ GeV.

Searches for RH neutrinos via SM mediated processes are being carried out at the LHC, including both prompt and displaced final states [3–11]. These searches currently put an upper limit of $|V_{\mu N}| \lesssim 10^{-3}$ on the active-sterile mixing with the muon and RH neutrino masses $m_N \lesssim 100$ GeV. The limits weaken rapidly for increasing heavy neutrino masses. This is expected because the SM W becomes increasingly off shell and thus the production cross section is doubly suppressed, from the active-sterile mixing as well as the mass of the heavy RH neutrino. Further projections for RH neutrinos from the SM production, at the LHC [12–38], the proposed SHiP detector [39,40], LHeC [41], and the FCC [22,24,42,43] have been carried out. These studies rely on the minimal and ensured RH neutrino production mechanism, taking advantage of higher luminosity, larger detectors, and increased center-of-mass energies. They remain fundamentally limited by the right-handed neutrino production cross-section suppressed by the active-sterile mixing. Together with the stringent cuts on the final state objects at FCC-hh, the studies show that probing the seesaw neutrino mass generation mechanism at future colliders via the minimal production channels will be very challenging.

This motivates the consideration of nonminimal models and probing neutrino mass generation mechanisms via

*wei.liu@njust.edu.cn; wei.liu.16@ucl.ac.uk
†suchita.kulkarni@uni-graz.at
‡f.deppisch@ucl.ac.uk

Published by the American Physical Society under the terms of the Creative Commons Attribution 4.0 International license. Further distribution of this work must maintain attribution to the author(s) and the published article's title, journal citation, and DOI. Funded by SCOAP³.

exotic production modes. In this context, the $B-L$ model offers an interesting avenue as it contains three additional heavy neutrino generation portals unsuppressed by the active-sterile mixing namely the heavy Z', heavy $B-L$ Higgs and the SM Higgs. There are two main advantages of these additional modes, especially for Z' mediated processes. First, the right-handed neutrinos can have large p_T depending on the Z' mass, which can be produced on shell. Second, given that this on shell Z' can be heavier than the W boson, right-handed neutrino masses $m_N \gtrsim 100$ GeV can be probed without penalizing production cross sections as opposed to the SM case where this mass range necessitates an off shell W mediator and leads to an additional suppression in cross section. These considerations enable searching for right-handed neutrinos in regions of $|V_{\mu N}|$ and m_N parameter space otherwise inaccessible. Analyses of $B-L$ processes have been performed in the literature. This includes reinterpretations of existing Z' production searches [44], analyses of the sensitivity at the lifetime frontier [45–48], explorations at the LHC [49–53], as well as prompt searches at the FCC-hh [54].

In this work, we look ahead and consider the potential of the FCC-hh detector at 100 TeV center-of-mass energy to probe right-handed neutrino production via the $B-L$ Z'. We contrast this mode with processes mediated by SM weak currents. In doing so, we not only exploit the gain in the center-of-mass energy and the higher luminosity (30 ab^{-1}), but also the larger detector volume capable of capturing longer lived right-handed neutrinos. In doing such an exercise our aim is to demonstrate the complementarity between SM weak current and $B-L$ mediated processes as well as to understand the prominent kinematic differences between FCC-hh and LHC, the two SM and $B-L$ channels. We consequently illustrate regions of parameter space that can be probed by simple analyses while highlighting the necessity to develop more comprehensive analysis techniques.

The paper is organized as follows: we begin by reviewing the $B-L$ gauge model and its immediate phenomenological consequences in Sec. II. This is followed by a discussion of our analysis setup in Sec. III. Using this as a basis, in Sec. IV we first evaluate the sensitivity of FCC-hh for Z' resonance production. We then discuss heavy neutrino production via SM W and $B-L$ Z' processes in Sec. V. We show our sensitivity estimates in Sec. VI and finally conclude in Sec. VII.

II. THE $B-L$ GAUGE MODEL

A. Model setup and particle spectrum

In addition to the particle content of the SM, the $U(1)_{B-L}$ model contains an Abelian gauge field B'_μ, a SM singlet scalar field χ, and three RH neutrinos $\nu_{R,i}$. The gauge group is $SU(3)_C \times SU(2)_L \times U(1)_Y \times U(1)_{B-L}$, where χ and N_i have $B-L$ charges $B-L=+2$ and -1, respectively. All SM particles carry their conventional $B-L$ quantum number. The scalar potential includes all terms allowed by the symmetry,

$$\mathcal{V}(H,\chi) = m^2 H^\dagger H + \mu^2|\chi|^2 + \lambda_1 (H^\dagger H)^2 + \lambda_2 |\chi|^4 + \lambda_3 H^\dagger H |\chi|^2, \tag{2.1}$$

with the SM Higgs doublet H. The scalar sector consists of a light SM-like Higgs $h_1 \sim h_0^{\rm SM}$ with $m_{h_1} \approx 125$ GeV and a heavy Higgs h_2 with $m_{h_2} \approx \sqrt{2\lambda_2}\langle\chi\rangle$. Here, $\langle\chi\rangle$ is the vacuum expectation value of the $B-L$ Higgs χ. The mixing between the Higgs fields, induced by the term λ_3 in Eq. (2.1), can still be sizeable but is not relevant for our discussion. We denote the gauge coupling strength associated with the $U(1)_{B-L}$ symmetry by g_{B-L}. In this paper, we neglect a kinetic mixing between the $U(1)_{B-L}$ and $U(1)_Y$ gauge bosons; i.e., we consider the minimal $B-L$ gauge model. Such a mixing will be generated radiatively even if assumed zero at, e.g., the $B-L$ breaking scale, $\epsilon(m_Z) \sim \frac{e g_{B-L}}{16\pi^2}\log(m^2_{Z'}/m^2_Z)$. This is negligible for our analysis. We note that a finite kinetic mixing can be beneficial in searching for heavy neutrinos. Its main effect will be that the SM Z can decay to two heavy neutrinos, suppressed by ϵ, but not by the active-sterile neutrino mixing. The mass of the Z' gauge boson is then simply given by $m_{Z'} = g_{B-L}\langle\chi\rangle$.

The model contains the additional Yukawa terms

$$\mathcal{L} \supset -y^\nu_{ij}\overline{L_i}\nu_{R,j}\tilde{H} - y^M_{ij}\overline{\nu^c_{R,i}}\nu_{R,j}\chi + \text{H.c.}, \tag{2.2}$$

where L_i are the SM lepton doublets, $\tilde{H} = i\sigma^2 H^*$, and a summation over the generation indices i, $j = 1, 2, 3$ is implied. The Yukawa matrices y^ν and y^M are *a priori* arbitrary. The RH neutrino masses are generated by breaking of the $B-L$ symmetry, with the mass matrix given by $M_R = \sqrt{2}y^M\langle\chi\rangle$. The light neutrinos mix with the RH neutrinos via the Dirac mass matrix $m_D = y^\nu v/\sqrt{2}$ where $v = \langle H^0\rangle \approx 246$ GeV is the SM Higgs vacuum expectation value. The combined 6×6 mass matrix in the (ν_L, ν^c_R) basis is then in block form

$$\mathcal{M} = \begin{pmatrix} 0 & m_D \\ m_D & M_R. \end{pmatrix}. \tag{2.3}$$

In the seesaw limit we consider, $\|M_R\| \gg \|m_D\|$, the light and heavy neutrino mass matrices are $m_\nu \sim -m_D \cdot M_R^{-1} \cdot m_D^T$ and $m_N \sim M_R$, respectively. The flavor $(\nu_{L,i}, \nu^c_{R,i})$ and mass (ν_i, N_i) eigenstates of the light and heavy neutrinos are connected in block form as

$$\begin{pmatrix} \nu_L \\ \nu^c_R \end{pmatrix} = \begin{pmatrix} V_{LL} & V_{LR} \\ V_{RL} & V_{RR} \end{pmatrix} \cdot \begin{pmatrix} \nu \\ N \end{pmatrix}. \tag{2.4}$$

The mixing matrix V_{LL} and the light neutrino masses are constrained by oscillation experiments to yield their observed values, i.e., the SM charged current lepton mixing $V_{LL} \approx U_{\rm PMNS}$ (apart from small nonunitarity corrections and taking the basis in which the charged lepton mass matrix is diagonal). The approximately unitary matrix V_{RR} describes the mixing among the RH neutrinos and the active-sterile mixing is $V_{LR} \approx m_D \cdot M_R^{-1}$.

We effectively consider the case of a single RH neutrino generation mixing with one SM neutrino at a time; specifically we focus on the mixing with the muon neutrino and hence take $V_{LL}, V_{RR} \sim 1$, and $V_{LR} \sim V_{\mu N}$ with active-sterile mixing strength $V_{\mu N}$ suppressing the charged-current interaction of the muon with the RH neutrino. We take the RH neutrino mass m_N and the mixing strength $V_{\mu N}$ as free model parameters. In order to generate a light neutrino mass $m_\nu \lesssim 0.1$ eV via the seesaw mechanism with $\|m_D\| \ll \|M_R\|$, the mixing strength takes the generic value

$$|V_{\mu N}| \approx \frac{m_D}{M_R} = \sqrt{\frac{m_\nu}{m_N}} = 10^{-6} \times \left(\frac{100\ \text{GeV}}{m_N}\right). \quad (2.5)$$

This is the generic expectation for the mixing strength of a single heavy Majorana neutrino generating a light neutrino mass of 0.1 eV. Both smaller and larger mixing is possible in more realistic and extended scenarios that incorporate all three generations of light neutrinos and at least two heavy neutrinos. Smaller mixing is possible by decoupling the heavy neutrino with other heavy neutrinos responsible for light neutrino mass generation. Larger mixing, up to current experimental constraints, is possible if there is cancellation among contributions of different heavy neutrinos. This can be achieved with either three generations of heavy neutrinos (see, e.g., [55]) or extended scenarios with quasi-Dirac heavy neutrinos, usually referred to as inverse seesaw.

B. Production and decay of heavy neutrinos

Within the $B-L$ model, heavy neutrinos can be produced at the FCC-hh via different mechanisms. The first and foremost are the SM mediators, i.e., the W and Z gauge bosons and the Higgs h_1. In addition, there are the $B-L$ mediators, namely the Z' gauge boson and the heavy Higgs boson h_2.

Out of these mechanisms, the SM Higgs production $pp \to h_1 \to NN$ will be suppressed by the Higgs mixing and the mass of the heavy neutrino with respect to the $B-L$ breaking scale, $m_N/\langle\chi\rangle$ ($m_N < m_{h_1}/2$) [29]. The alternative mode $pp \to h_1 \to N\nu$ is instead suppressed by the active-sterile neutrino mixing. The production via the heavy Higgs h_2, $pp \to h_2 \to NN$, is possible as well but likewise suppressed by $m_N/\langle\chi\rangle$, though higher neutrino masses can be probed. The mode $pp \to h_2 \to N\nu$ is suppressed by both the Higgs and the active-sterile neutrino mixing.

The best studied SM modes are via the W and Z gauge bosons, $pp \to W \to N\ell$ and $pp \to Z \to N\nu$. They are generally suppressed by the active-sterile neutrino mixing and for $m_N > m_W, m_Z$ proceed through off shell gauge bosons with further strong suppression for high N masses. The W mediated channel gives rise to a prompt lepton, which helps in accepting events even if the heavy neutrino decays via a displaced vertex. We will thus focus on this mode.

Finally, the main production mode in our analysis is via the $B-L$ Z' gauge boson, $pp \to Z' \to NN$. The production cross section $\sigma(pp \to Z')$ at the LHC and FCC-hh is shown in Fig. 3 (left) in Sec. IV to determine the reasonable range of the gauge coupling g_{B-L} at the FCC-hh era. The partial decay width of $Z' \to NN$ per generation of heavy neutrino is

$$\Gamma(Z' \to NN) = g_{B-L}^2 \frac{m_{Z'}}{24\pi}\left(1 - \frac{4m_N^2}{m_{Z'}^2}\right)^{3/2}. \quad (2.6)$$

Considering the Z' to be much heavier than the SM fermions into which it decays, the total decay width is

$$\Gamma(Z') \approx g_{B-L}^2 \frac{m_{Z'}}{24\pi}\left[13 + 3\left(1 - \frac{4m_N^2}{m_{Z'}^2}\right)^{3/2}\right], \quad (2.7)$$

with three generations of heavy neutrinos.

In all mechanisms we must then consider the decays of the heavy neutrino. They proceed via the same mediators as discussed above. The h_1, h_2 mediated decays are suppressed by the Yukawa coupling $\sim m_N/\langle\chi\rangle$ and the heavy neutrino dominantly decays via SM W and Z, $N \to W^{(*)}\ell, Z^{(*)}\nu$. We do not consider decays via Z' such as $N_2 \to Z'N_1$ as we take into account only a single generation of heavy neutrino. In any case the gauge boson mediated decay widths are suppressed by the active-sterile mixing.

For heavy neutrino masses $m_N \lesssim m_W, m_Z$, decays will take place via off shell W and Z. The branching ratios of such light heavy neutrinos are discussed in [29,56]. If the heavy neutrino mass is above this threshold, two body decays via on shell W, Z occur. The heavy neutrino branching ratios in such cases are approximately independent of the mass and $\text{BR}(N \to W\ell) \approx 70\%$ while $\text{BR}(N \to Z\nu) \approx 30\%$. Considering decays through a single SM lepton generation, the branching ratios are also independent of the active-sterile mixing.

With the SM W and Z decaying further, the N decays can thus result in $N \to \ell^+\ell^-\nu$ corresponding to the $W^{(*)}$ and $Z^{(*)}$ mediated leptonic decays with visible final states. Finally, we also get $N \to \ell jj$, which corresponds to the hadronic W, Z decays.

With the assumption of flavor-diagonal active-sterile neutrino mixing, we concentrate on one generation of heavy neutrinos, namely coupling to muons and muon

neutrinos. Out of the several final states it can produce we will in particular consider $N \to \mu\mu\nu$, $N \to \mu jj$ for neutrino masses lighter than 100 GeV and $N \to \mu W \to \mu\mu\nu$, $N \to \mu W \to \mu jj$ for heavier neutrinos. We concentrate on muon flavor as muon performance in several parts of the detector is generally expected to be superior and we consider the μjj final state as it has a larger branching ratio.

While the branching ratios are largely independent of the heavy neutrino mass and the active-sterile neutrino mixing, the total decay width and thus the decay length crucially depend on it. For $m_N \lesssim m_Z$, the proper decay length can be approximated as [56]

$$L_N^0 \approx 2.5 \text{ cm} \times \left(\frac{10^{-6}}{|V_{\mu N}|}\right)^2 \times \left(\frac{100 \text{ GeV}}{m_N}\right)^5. \quad (2.8)$$

For $m_N \gtrsim 100$ GeV, decays are proportionally faster due to their on shell nature. Approximately, the proper decay length in this regime is [56]

$$L_N^0 \approx 0.1 \text{ mm} \times \left(\frac{10^{-6}}{|V_{\mu N}|}\right)^2 \times \left(\frac{100 \text{ GeV}}{m_N}\right)^3. \quad (2.9)$$

III. ANALYSIS SETUP

A. FCC-hh detector geometry

The future physics collider program has two major goals; first and foremost to measure the SM Higgs boson and SM electroweak sector properties as precisely as possible and a second to search for and potentially discover new physics

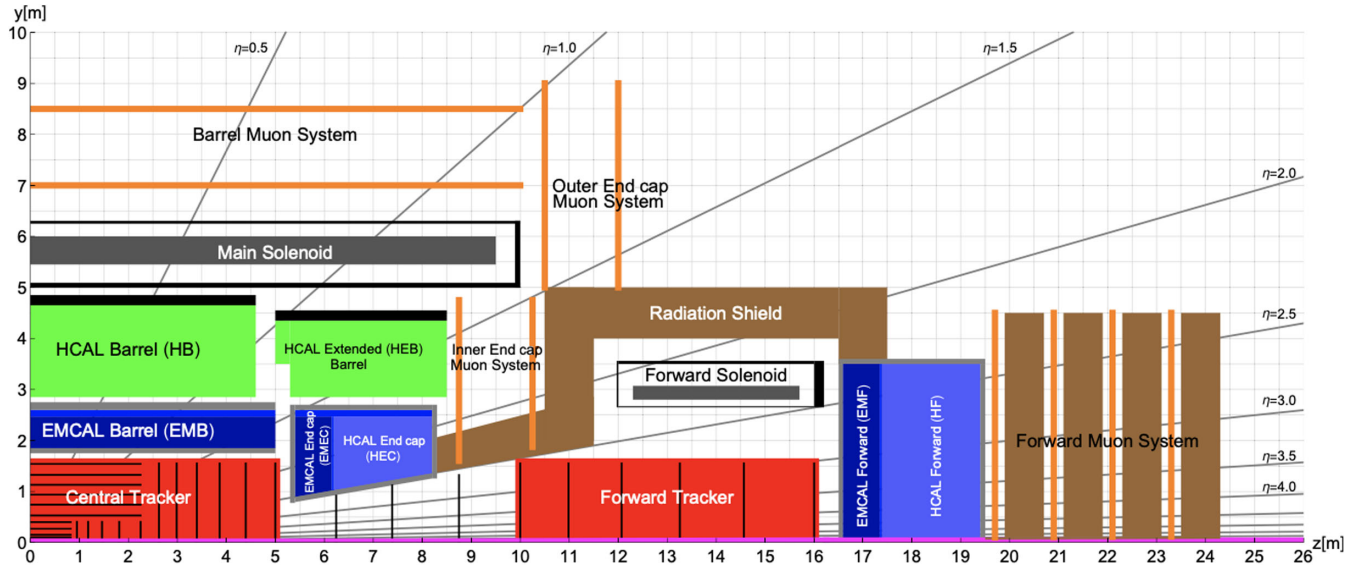

FIG. 1. Longitudinal cross section of the FCC-hh reference detector. Taken from [57].

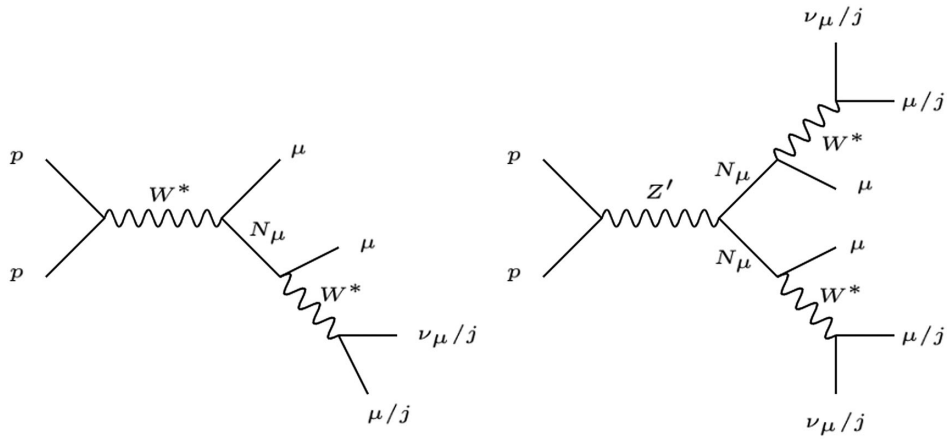

FIG. 2. Feynman diagram of the SM W production of the heavy neutrino, $pp \to W^* \to N_\mu \mu$ (left) and Z' production of the heavy neutrino, $pp \to Z' \to NN$ (right).

TABLE I. Different final states arising from prompt decays of heavy neutrinos for SM and $B-L$ mediated production mechanism.

Category	Decay chain	Final state
SM	$pp \to W^* \to \mu N; N \to \mu\mu\nu$	$3\mu + \not{E}_T$
SM	$pp \to W^* \to \mu N; N \to \mu jj$	$2\mu + 2j$ (OS/SS)
$B-L$	$pp \to Z' \to NN; N \to \mu jj; N \to \mu jj$	$2\mu + 4j$ (OS/SS)
$B-L$	$pp \to Z' \to NN; N \to \mu jj; N \to \mu\mu\nu$	$3\mu + 2j + \not{E}_T$
$B-L$	$pp \to Z' \to NN; N \to \mu\mu\nu; N \to \mu\mu\nu$	$4\mu + \not{E}_T$
SM	$pp \to W^* \to \mu N; N \to \mu\mu\nu$	$\mu^{\text{prompt}} + 2\mu^{\text{disp}}$
SM	$pp \to W^* \to \mu N; N \to \mu jj$	$\mu^{\text{prompt}} + (\mu jj)^{\text{disp}}$
$B-L$	$pp \to Z \to NN; N \to \mu\mu\nu;$ $N \to$ inclusive	$2\mu^{\text{disp}}$
$B-L$	$pp \to Z \to NN; N \to \mu jj;$ $N \to$ inclusive	$(\mu jj)^{\text{disp}}$

that may be out of reach at the LHC. A two stage plan is proposed towards fulfilling these goals. The first stage is an electron-positron collider with a center-of-mass collision energy of 240 GeV called the FCC-ee.[1] The second will be a hadron-hadron collider with a center-of-mass collision energy of 100 TeV and an integrated luminosity of at least 10 times larger of the HL-LHC, i.e., 30 ab^{-1} [57]. In this paper, we focus on the reach of FCC-hh for a BSM particle, the heavy neutrino, therefore, we briefly discuss below the FCC-hh geometry.

Due to the high center-of-mass energy, the FCC-hh can in general produce boosted objects, therefore the FCC-hh detector is being designed to accept high pseudorapidities $|\eta| \lesssim 4$. The detector subcomponents and geometry are shown in Fig. 1, taken from Ref. [57]. As detailed below we implement this geometry in our analysis in order to account for geometrical acceptance. Compared to the LHC detector, the FCC-detector is larger both in longitudinal and transverse directions in order to capture higher energy final states. The larger volume is of a particular importance in detecting long-lived particles as larger lifetimes can be probed.

In order to estimate the potential of the FCC-hh detector to probe displaced final states, we consider a fiducial volume of the detector, in particular the following regions [57]:

(i) Inner tracker: $0.025\text{m} < L_{xy} < 1.55$ m and $L_z < 5$ m,
(ii) Region 2 (calorimeter): $1.7\text{m} < L_{xy} < 7\text{m}$ and $L_z < 9\text{m}$,
(iii) Forward tracker: $2.5 < |\eta| < 4$, $0.025\text{ m} < L_{xy} < 1.55$ m and $10\text{ m} < L_z < 16$ m,
(iv) Forward region 2 (calorimeter): $2.5 < |\eta| < 4$, $0.025\text{ m} < L_{xy} < 4$ m and $16.5\text{ m} < L_z < 19.5$ m.

Here L_{xy} and L_z are the transverse and perpendicular displacements, respectively. We consider a decay prompt if $L_N \leq 1$ mm [57]. This is possible either when the mixing $|V_{\mu N}|$ is large or $m_N > 100$ GeV, irrespective of the SM or $B-L$ mediated production channels.

[1]In addition, there will also be a run at the Z pole with luminosity larger than the LEP luminosity.

B. Signal final states

A number of different final states are possible depending on the production and decay of the heavy neutrino. We show the corresponding Feynman diagrams in Fig. 2, which includes the full production and decay chain for the RH neutrinos we consider in this work. The corresponding final states are summarized in Table I. In general they contain a combination of muons, jets, and missing energy. We separate the processes depending on the production mechanism, i.e., SM or $B-L$, and also on the prompt or displaced category. Among the prompt production, five different final states are possible. Out of these final states, within this analysis we will not consider $3\mu + 2j + \not{E}_T$ final state.

We foresee a signal-background discrimination on the basis of missing energy where available. When missing energy is not available, we will demonstrate the use of same sign (SS) or opposite sign (OS) muons in the final state. Later on we will explicitly demonstrate the effectiveness of these strategies to derive the final sensitivity. For the displaced final states, we will consider an inclusive analysis considering either one prompt lepton and one displaced vertex originating out of two displaced muons (for SM mediated heavy neutrino production), or one displaced vertex forming out of two displaced muons (for $B-L$ mediated production).

In order to trigger on this signal, we use either a single prompt or displaced lepton trigger. In accordance with the FCC-hh Conceptual Design Report [57], we require the leading muon p_T greater than 150 GeV mimicking a trigger strategy. For a displaced muon trigger, no concrete numbers are as yet available, however we increase the p_T cut by a factor 1.5 in order to keep in line with the experience of dealing with displaced versus prompt objects at the

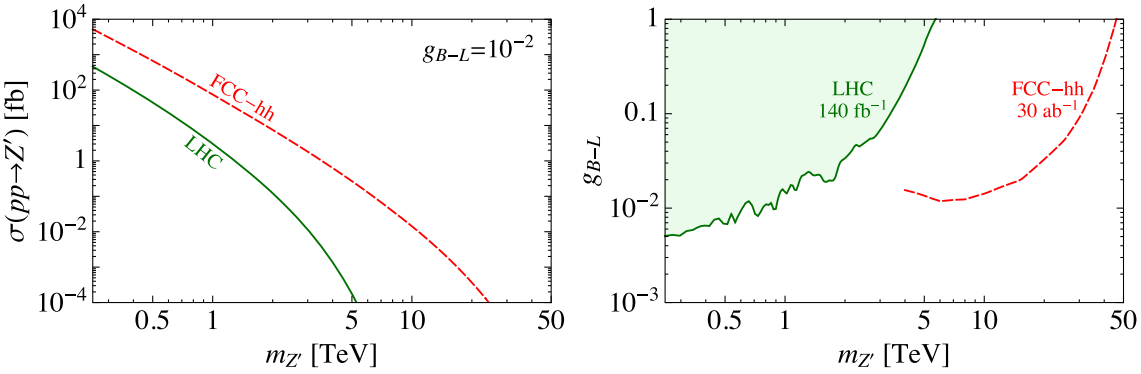

FIG. 3. Left: cross section $\sigma(pp \to Z')$ as a function of the Z' gauge boson mass $m_{Z'}$ at the 13 TeV LHC and 100 TeV FCC-hh with $g_{B-L} = 10^{-2}$. Right: upper limit on the $U(1)_{B-L}$ gauge coupling g_{B-L} as a function of $m_{Z'}$ at the LHC with 140 fb^{-1} luminosity (green) [58,59] and projected sensitivity at the FCC-hh with 30 ab^{-1} (red dashed), recast from [60].

LHC [61]. Thus, for a displaced muon final state, we require a leading displaced muon with $p_T(\mu_1) > 200$ GeV.

C. Simulation details

To analyze the kinematics and later on sensitivity, we simulate the signal events using the following steps. We use the universal FeynRules output (UFO) [62] of $B-L$ model developed in Ref. [29] in combination with the Monte Carlo event generator MadGraph5aMC@NLO-v2.6.7 [63] at parton level. The FeynRules [64,65] model file and UFO is publicly available from the FeynRules Model Database at [66]. For every signal sample, we generate 10^4 signal events. We then pass the generated parton level events on to PYTHIA V8.235 [67] which handles the initial and final state parton shower, hadronization, heavy hadron decays, etc. The clustering of the events is performed by FastJet v3.2.1 [68].[2] Additionally, we use the `NNPDF23_lo_as_0130_qed` PDF set. Using the same setup we also produce 10^5 background events in each $t\bar{t}$ (leptonic), ZWW (leptonic), and $\mu\nu Z$ (leptonic) final states. In particular, we consider only muon flavored final states for backgrounds that will be compatible with our signal final states.

Finally in order to minimize the Monte Carlo efforts, heavy neutrinos are always decayed promptly. We simulate displacement via inverse sampling of the decay distribution. Specifically, the efficiency of our displaced vertex analysis relies on both the geometrical acceptance of the detector, ϵ_{geo}, as well as the reconstruction effects, ϵ_{recon}, and the total efficiency is $\epsilon_{\text{DV}} = \epsilon_{\text{geo}} \times \epsilon_{\text{recon}}$. The geometrical acceptance of the detector includes the probability of the heavy neutrino traveling a distance L from the interaction point before decaying, given by the exponential density distribution

$$p(L)dL = \frac{dL}{L_N} e^{-L/L_N}, \tag{3.1}$$

where L_N is the decay length of the boosted heavy neutrino in the laboratory frame. The efficiency ϵ_{geo} is calculated by inverse sampling of the cumulative decay length distribution function, which in turn depends on the heavy neutrino mass and boost, and the active-sterile mixing. The reconstruction efficiency is assumed $\epsilon_{\text{recon}} = 100\%$ unless otherwise stated.

IV. FCC-hh REACH FOR HEAVY Z' PRODUCTION

Before we proceed, we estimate the FCC and LHC potential to probe Z' resonance mass. A detailed investigation of low mass Z' production mechanisms and LHC limits was carried out in [69,70]. In this study, we are instead interested in high mass Z' and the associated experimental sensitivity. To this end we exploit the existing CMS resonance search in dilepton final state at 140 fb^{-1} luminosity [58]. Comparable results can be obtained by recasting the ATLAS search in the same final state [71]. We furthermore compliment these limits with the projected FCC-hh limits as detailed in [60]. We recast both these limits for the $B-L$ coupling. The recast is performed as follows. We calculate the simulated cross section $\sigma^{\text{ref}}(pp \to Z' \to l\bar{l})$ using the $B-L$ model UFO with fixed g^{ref}_{B-L} without implementing any generator cuts, then we require the cross section $\sigma(\text{U.L.})$ to be equal to the upper limits from the Ref. [58], therefore $(g^{\text{U.L.}}_{B-L})^2/(g^{\text{ref}}_{B-L})^2 \times \sigma^{\text{ref}}(pp \to Z' \to l\bar{l}) \sim \sigma(\text{U.L.})$.

In Fig. 3, we show the resulting Z' production cross section (left panel) and the limits on the g_{B-L} coupling (right panel) at HL-LHC (green) and FCC-hh (red), respectively. Comparing the Z' production cross section (left panel) between HL-LHC and FCC-hh, it is clear that FCC-hh will gain significant cross section for the production of heavier Z', thus extending the reach for heavier resonances.

[2]When analyzing the hadron level events, we remove the muons from the N decays in the genjets collection.

This gain in cross section is complemented by a large luminosity of 30 ab^{-1}, and they are in turn reflected in the more stringent g_{B-L} limits (right panel). Starting from about $m_{Z'} = 4$ TeV the FCC-hh will improve the g_{B-L} limit by at least an order of magnitude. The lack of significant gain at low Z' masses is due to the large dilepton background at the FCC-hh [60]. This background becomes much smaller at high mass, and correspondingly high mass resonances can be probed. For Z' lighter than ∼4 TeV, the Z' decays to heavy neutrinos can lead to displaced final states and may be beneficial for exploring lower Z' mass due to smaller backgrounds. We will not explore this region any further however such a strategy might be worth exploring further.

It is thus clear that FCC-hh will in general be able to produce much heavier Z' as compared to HL-LHC and correspondingly improve the limits on g_{B-L}. This has important implications for the heavy neutrinos produced via Z'. First and foremost, the heavy neutrino will in general be produced with a large boost which will produce more energetic decay products in the final state. Second, such large boosts will result in longer decay lengths of the heavy neutrinos producing more displaced objects in the detector.

We require $\sigma(pp \to Z') > 10^{-2}$ fb in order to achieve ∼10 signal events $Z' \to NN$ final state at 30 ab^{-1}. Considering the FCC-hh's reach as shown in Fig. 3, we assume a benchmark point of $m_{Z'} = 5$ TeV and $g_{B-L} = 10^{-2}$ in the rest of the paper.

V. HEAVY NEUTRINO PRODUCTION AT THE FCC-hh

Having understood the reach of the FCC-hh in terms of the Z' mass and gauge coupling, we are now equipped to compute the heavy neutrino production cross section and decay modes. To this end, we explore the heavy neutrino production via the SM W, Z mediators and via the $B-L$ Z'. We furthermore also demonstrate effect of p_T cut on leading lepton, in accordance with our trigger strategy. We simulate these processes as discussed in Sec. III C.

A. Heavy neutrino production via SM W boson

The production of heavy neutrinos from SM W, Z bosons will always remain primary mechanism as it only relies on the active-sterile mixing naturally expected to generate neutrino masses. In this section we will illustrate the heavy neutrino production cross sections from both W and Z mediators; however for our final analysis we will consider only the W mediated process and use the $\mu\mu\nu$ or μjj final state from the decay of the heavy neutrinos to assess the sensitivity. Among the lepton final states, only muon flavor is considered as it is cleaner and in general leads to higher detector efficiency compared to electrons or taus.

Benefiting from the 100 TeV collision energy, the cross section of the Drell-Yan process $pp \to W^{\pm} \to \mu^{\pm}\nu$ will increase from 1.56×10^7 fb at the 13 TeV LHC to 1.05×10^8 fb at the 100 TeV FCC-hh.

B. Heavy neutrino production via Z' boson

In the case of heavy neutrino production via a Z' mediator, the production cross section is given by $\sigma(pp \to Z') \times \mathrm{BR}(Z' \to NN)$ [47], where the branching ratio is independent of the active-sterile mixing.

Assuming a 5 TeV Z' gauge boson, with $g_{B-L} \sim 10^{-2}$, which saturates the FCC-hh sensitivity and $m_N \sim 10$ GeV, the $pp \to Z' \to NN$ cross section reaches $\sim 10^{-2}$ fb. This cross section will be approximately constant up to $m_N = 2.5$ TeV, beyond which it will vanish due to phase space considerations.

In order to understand the complementarity of $B-L$ heavy neutrino production with the SM mediated production processes, we compare the two cross sections before and after imposing the cut $p_T(\mu_1) > 150$ GeV, consistent with the trigger requirement. In Fig. 4 (left), we show the heavy neutrino production cross sections via SM W, Z, as well as $B-L$ Z' with $N \to \mu^+\mu^-\nu$ for $|V_{\mu N}| = 10^{-2}$, $g_{B-L} = 10^{-2}$ and $m_{Z'} = 5$ TeV (left panel). For the Z' mediated process, only one of the two heavy neutrinos decays. We also show contours of 1 ab production cross section as a function of heavy neutrino mass and mixing angle (right panel).

Several features of these plots are to be noticed: First, the production cross sections via SM mediators should be rescaled by the ratio of the square of the mixing angles for $|V_{\mu N}| \neq 10^{-2}$. Such rescaling does not apply for the Z' channel. Therefore, although for $|V_{\mu N}| = 10^{-2}$, the SM mediated production cross section is much larger than the Z' counterpart, for smaller mixing angles the situation will be reversed. The crossover between Z' and SM W mediated channels takes place for $|V_{\mu N}| \sim 10^{-5}$ without the p_T cut, and for $|V_{\mu N}| \sim 10^{-3}$ after the cut. Second, the effect of the p_T cut is much stronger on the SM mediated channel, while for the Z' mediated process there is virtually no effect of the p_T cut. This is because the heavy Z' mass already leads to energetic displaced leptons in the final state, the lighter W and Z on the contrary lead to softer prompt leptons. As can be seen from the plot, the cross section via SM mediators can drop by three order magnitude after such a lepton p_T cut. Finally, the SM Z mediated cross section is approximately one order magnitude smaller than the corresponding W mediated process, which justifies our decision to neglect the Z mediated processes.

C. Kinematics of the heavy neutrino and its final states

Having explained the heavy neutrino production cross sections in the previous section, we also discuss the kinematics of the final states by considering the two production

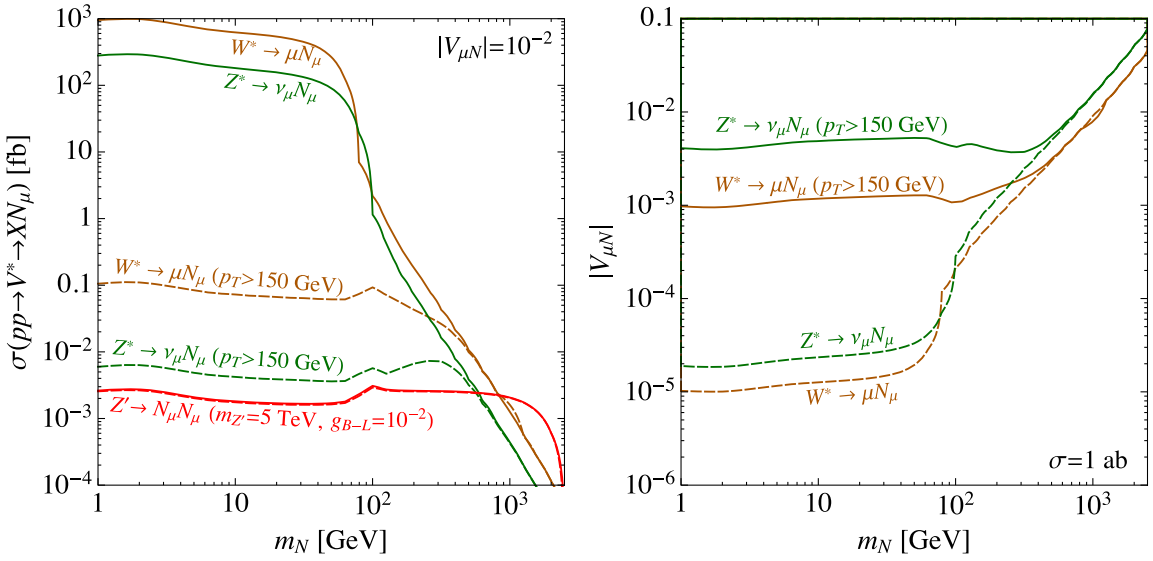

FIG. 4. Left: production cross sections of $pp \to W^\pm \to Nl^\pm, N \to \mu^+\mu^-\nu$ (orange), $pp \to Z \to N\nu, N \to \mu^+\mu^-\nu$ (green), and $pp \to Z' \to NN, N \to \mu^+\mu^-\nu$ (red) as functions of m_N at the 100 TeV FCC-hh. The solid curves are before cuts and the dashed curves are after applying the leading $p_T(\mu) > 150$ GeV cut. The active-sterile mixing is fixed at $|V_{\mu N}| = 10^{-2}$. Right: contours of heavy neutrino production cross section at 1 ab in the $(m_N, |V_{\mu N}|)$ plane at the 100 TeV FCC-hh. The curves correspond to SM production channels before (solid) and after (dashed) the p_T cut on final state leptons.

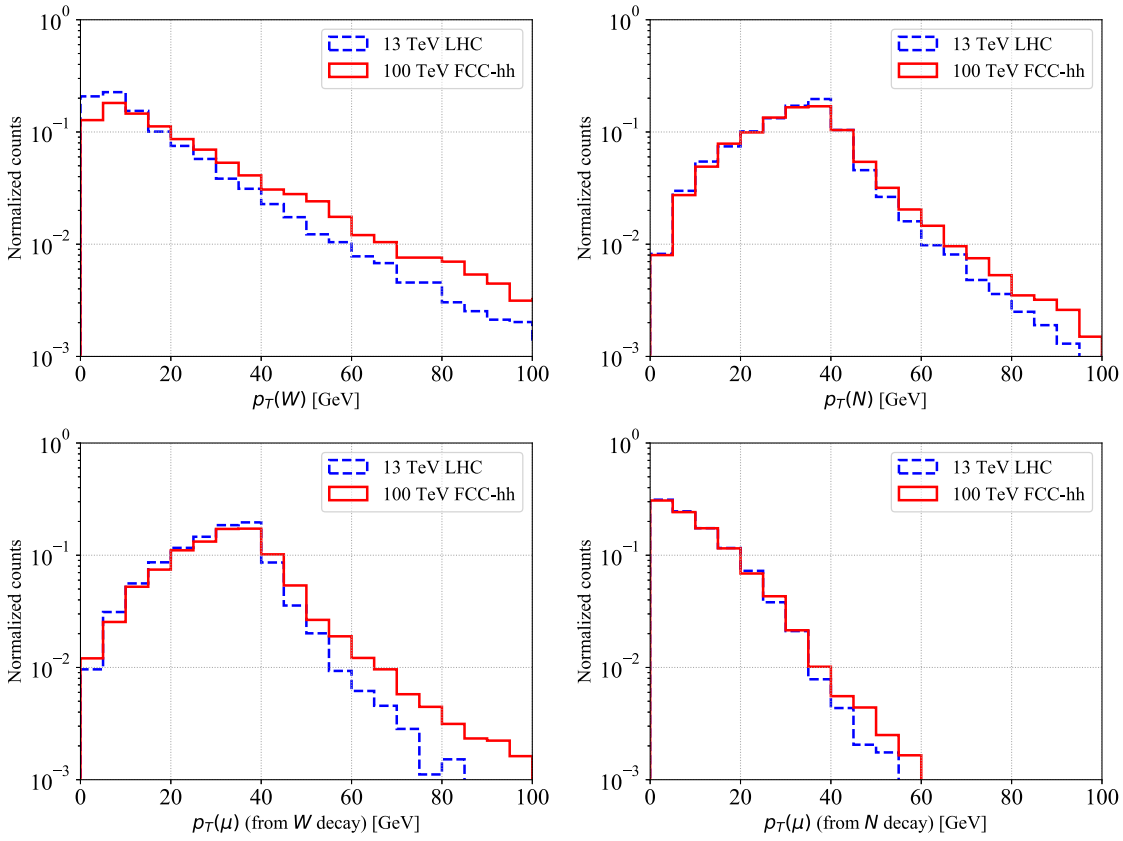

FIG. 5. Transverse momentum distribution of particles in the process $pp \to W^\pm \to N\mu^\pm, N \to \mu\mu\nu$: $p_T(W)$ (upper left panel), $p_T(N)$ (upper right panel), $p_T(\mu)$ from the W boson decay (bottom left panel), and $p_T(\mu)$ from the N decay (bottom right panel) at the 13 TeV LHC (blue dashed) and 100 TeV FCC-hh (red solid).

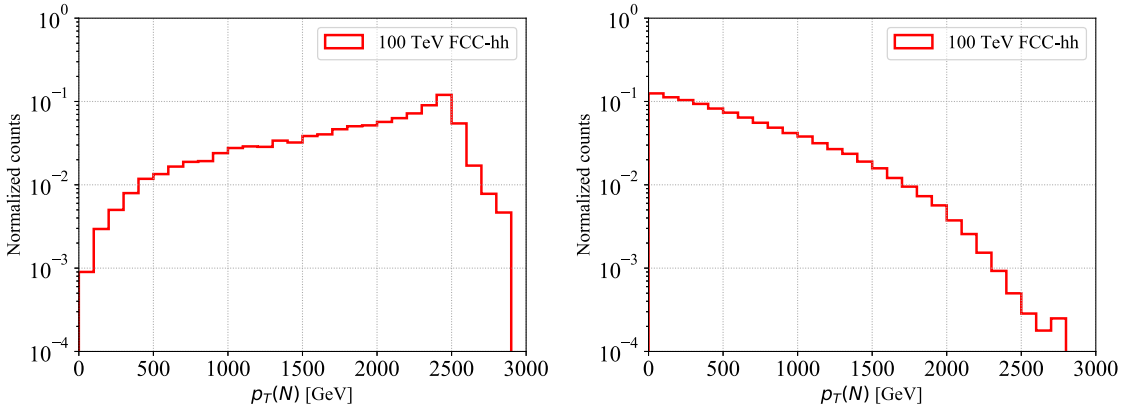

FIG. 6. Left: $p_T(N)$ in the $pp \to Z' \to NN$ process at the FCC-hh. Right: $p_T(\mu)$ from the N decay.

channels of the heavy neutrinos either via a SM W or $B-L$ Z'. For the final states, we only take $N \to \mu^+\mu^-\nu$ as an example. We compare the p_T distributions of the resulting heavy neutrino, muons, and $W^{(*)}$ to illustrate advantages of each of the production modes.

For the SM mediated production, we compare the kinematics between LHC and FCC-hh center of mass energies. In Fig. 5 (top row), we plot the p_T of the mediator $W^{(*)}$ (left panel) and N (right panel) in $pp \to W^{(*)} \to N\mu$ at the 13 TeV LHC (blue dashed) and FCC-hh (red solid). As the $W^{(*)}$ boson is produced in the s channel, it has a small transverse momentum. In the left panel, with larger energy, the average of the $p_T(W^{(*)})$ increases by a few GeV at the FCC-hh, while most of the $W^{(*)}$ bosons still possess vanishing p_T. Correspondingly, as shown in Fig. 5 (right) the heavy neutrino p_T does not increase significantly at the FCC-hh as compared to the LHC. The gain in sensitivity at the FCC-hh is therefore primarily due to the larger production cross section.

In Fig. 5 (bottom row), we plot the p_T of the (prompt) muon from $W^{(*)}$ and from N decays. We fix the mass of the heavy neutrino to 10 GeV for concreteness. As the $W^{(*)}$ or the N do not gain significant energy at the FCC-hh as compared to the LHC, the resulting final states also do not gain any more p_T, as reflected in the muon p_T distributions shown. As we will see later, for this reason, FCC-hh does not lead to a large gain in sensitivity for SM mediated heavy neutrino production.

In contrast to the SM production, the heavy neutrinos in $B-L$ production can have significant p_T, as they are produced from a heavy resonance, i.e., a 5 TeV Z' (as shown in Fig. 6, left). Therefore, in $N \to \mu\mu\nu$ decay, the final μ can have $p_T \sim \mathcal{O}(100)$ GeV (see Fig. 6, right). It thus becomes easier to pass the stringent p_T requirements, e.g., for trigger purposes. However, due to the presence of the heavy Z', it is also possible that the decay products of the heavy neutrino are collimated.

To illustrate this, in Fig. 7 (left), we plot the ΔR between the final state muons (and jet) for the leptonic N decay ($N \to \mu\mu\nu$) for three heavy neutrino masses of 1 GeV (solid line), 10 GeV (dotted line), and 100 GeV (dashed line). We analyze here decays of only one of the heavy neutrinos. In principle, larger muon multiplicities can be obtained if decays of the second heavy neutrino are also considered. Such muons coming from two different heavy neutrinos

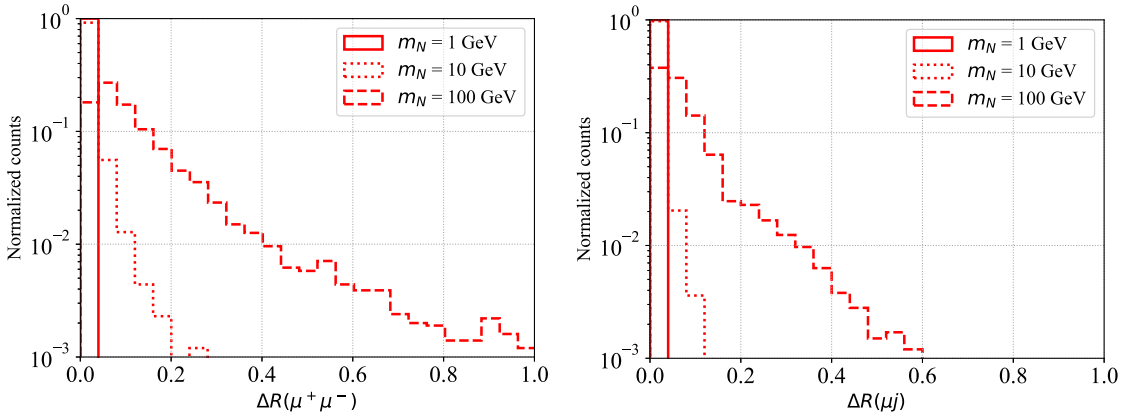

FIG. 7. Left: $\Delta R(\mu^+\mu^-)$ from $pp \to Z' \to NN, N \to \mu\mu\nu$ for $m_N = 1$, 10, 100 GeV. Right: $\Delta R(\mu j)$ from the $pp \to Z' \to NN, N \to \mu jj$ for $m_N = 1$, 10, 100 GeV. $m_{Z'}$ is fixed at 5 TeV. All distributions are shown for FCC-hh.

will however not lead to a vertex and hence can be discarded. We therefore assume that only one heavy neutrino decays to illustrate potentially nonisolated muons. From these distributions it is clear that muons can be very collimated when the mass difference between Z' and heavy neutrino is large. To demonstrate a similar situation in the semileptonic decay ($N \to \mu jj$), in Fig. 7 (right) we plot the minimum ΔR between the muon and two of the jets emerging from $N \to \mu jj$. In order to remove any soft hadronic activity in the event we consider jets with $p_T > 100$ GeV. It can be seen that for heavy neutrinos lighter than 10 GeV, the ΔR is smaller than 0.2. This poses potential isolation problems in leptonic final states and can also lead to fat jets in hadronic final states.

VI. SENSITIVITY

We now estimate the sensitivity of the FCC-hh with 30 ab^{-1} integrated luminosity to heavy neutrino production both via SM W and $B - L$ Z' mediators. For each of these production modes we consider two different heavy neutrino decay channels, namely $\mu\mu\nu$ and μjj, which correspond to either the leptonic or hadronic W decay. For the SM W mediated mode, we always use the prompt lepton as a trigger. For the $B - L$ Z' mode, we use the prompt and the displaced lepton triggers. We furthermore consider any RH neutrino decaying within the detector volume as outlined in Sec. III A and $L_N > 1$ mm as displaced.

Before we calculate the sensitivity, an estimation of the background is necessary. In general, this analysis can be carried out in several categories depending on charge and flavor composition of the signal processes (see [42] for such an exercise for SM mediated heavy neutrino production). We however restrict ourselves to muons in the final state and consider either same sign or opposite sign muons when a sufficient number of signal events are available. Unsurprisingly, the charge composition is relevant only when the signal originates from semileptonic decays of a heavy neutrino (μjj final state). As indicated before, the main signal and background discriminating variables we use are missing energy, the number of jets, the lepton charge composition, and the invariant mass of the system. These are summarized in Table II. In Table III, we show the main background processes and approximate number of

TABLE II. Different cuts on final states for various prompt signal categories considered.

	$3\mu + \not{E}_T$	$2\mu + 2j$	$2\mu + 4j$	$4\mu + \not{E}_T$
		(OS/SS)	(OS/SS)	
Common cuts		$p_T(\mu_1) > 150$ GeV, $p_T(\mu) > 20$ GeV, $p_T(j) > 20$ GeV, $\lvert\eta(\mu, j)\rvert \leq 4$		
Lepton charge		$\mu^+\mu^-/\mu^\pm\mu^\pm$	$\mu^+\mu^-/\mu^\pm\mu^\pm$	
Number of light jets	0	$= 2$	$= 4$	0
b-jet veto	No	Yes	Yes	No
$\not{E}_T$		< 20 GeV	< 20 GeV	> 100 GeV
M_{inv}		> 4 TeV	> 4 TeV	

TABLE III. Main background processes and their approximate number of events for the corresponding signal at the FCC-hh with 30 ab^{-1} integrated luminosity. The cuts $p_T > 150(20)$ GeV for the leading (subleading) muon and $p_T > 20$ GeV for jets are put. The number of leptons and jets are required to match the signal. In addition, $\not{E}_T > 100$ GeV is put for ZZZ background to cut out the ones from ZZ. And $\not{E}_T < 20$ GeV with b-tag veto with an efficiency of 0.3 for each jet, and $\mathrm{M}(t\bar{t}) > 4$ TeV are applied for the $t\bar{t}$ [42].

SM Prompt	Background	σ(fb)	$\mathrm{M}(t\bar{t})$	N_{B}
Leptonic ($\mu\mu\mu\not{E}_T$)	$\mu^\pm\nu Z$	11.9	$\cdots$	3.55×10^5
Hadronic OS ($\mu^\pm\mu^\mp jj$)	$t\bar{t}$ (leptonic decay)	1.84	$\cdots$	5.52×10^4
Hadronic SS ($\mu^\pm\mu^\pm jj$)	$t\bar{t}$ (leptonic decay)	1.84×10^{-3}	$\cdots$	55.2
$B - L$ prompt	Background	σ(fb)	$\mathrm{M}(t\bar{t})$	N_{B}
Leptonic ($\mu\mu\mu\mu\not{E}_T$)	ZWW	5.92×10^{-2}	$\cdots$	1.78×10^3
Hadronic OS ($\mu^\pm\mu^\mp jjjj$)	$t\bar{t}$ (leptonic decay)	1.85	8.73×10^{-2}	2.62×10^3
Hadronic SS ($\mu^\pm\mu^\pm jjjj$)	$t\bar{t}$ (leptonic decay)	1.85×10^{-3}	Negligible	Negligible
Displaced vertex	Background	σ(fb)	$\mathrm{M}(t\bar{t})$	N_{B}
Leptonic ($\mu\mu\not{E}_T$)	$\cdots$	$\cdots$	$\cdots$	Negligible
Hadronic (μjj)	$\cdots$	$\cdots$	$\cdots$	Negligible

expected events for a luminosity of 30 ab^{-1} after respective cuts.

We begin by discussing background composition and reduction methodologies for SM mediated heavy neutrino production and prompt decays. For heavy neutrino decays to muonic final states ($\mu\mu\mu\nu$), the background consists of $\mu^{\pm}\nu Z$ with leptonic Z decays. This background has approximately 10^5 events, therefore we require $\sim 10^3$ signal events. It should be noted that we attempt no optimization in terms of final state flavor composition. For the hadronic final state ($\mu\mu jj$), $t\bar{t}$ backgrounds are dominant. As the signal contains a fully visible final state, the resulting missing energy is small. Therefore, missing energy is a relevant discriminator here. For the opposite sign muons category requiring $p_T(\mu_1) > 150$ GeV, $\not{E}_T < 20$ GeV and putting a b-jet veto on the leptonic $t\bar{t}$ decays leads to $\sim 10^4$ events. Requiring same sign leptons (muons) in the final state leads to a more promising situation where backgrounds emerge from charge misidentification. Assuming an optimistic rate of 0.1% based on LHC detector performance [72] leads to ~ 10 events [42].

For the prompt final states of the $B-L$ mediated processes, two heavy neutrinos are produced. The signal final states we concentrate on are leptonic decays of both heavy neutrinos ($4\mu + \text{MET}$) and semileptonic decays of both heavy neutrinos ($2\mu + 4j$).[3] For $4\mu + \text{MET}$ final state, triple boson background processes (ZWW) have $\sim 10^3$ events. For the $2\mu + 4j$ final state, the $t\bar{t}$ mode in opposite sign muon and same sign muon final states are controlled by requiring low missing energy $\not{E}_T < 20$ GeV and high invariant mass $M(t\bar{t}) > 4$ TeV. For the opposite sign final states, there are still $\sim 10^3$ background events after the cuts, while they become negligible after additionally requiring charge misidentification for the same sign final states.

Finally, for the displaced final states, in the case of SM W mediated production, we always use the available prompt lepton with a $p_T > 150$ GeV to emulate the trigger and require either two displaced muons, in the case of $N \to \mu\mu\nu$ decays, or one displaced muon and one jet, for $N \to \mu jj$ decays. In addition, we require that the heavy neutrino decays within the detector volume, with geometry as described in Sec. III A. We consider the background to be negligible as the signal is sufficiently displaced [73–75], and only $N_{\text{signal}} > 3.09$ is required from the Poisson distribution at 95% confidence level (CL).

The resulting sensitivity at 95% CL is shown in Fig. 8, for the $\mu\mu\nu$ channel. For Z' mediated production, we fix $m_{Z'} = 5$ TeV, while taking the $B-L$ coupling at two representative values, $g_{B-L} = 10^{-2}$ and 0.1, reflecting either a pessimistic view that the g_{B-L} is taken near the projected sensitivity of the FCC-hh or an optimistic view with g_{B-L} as large but satisfying the current LHC limits.

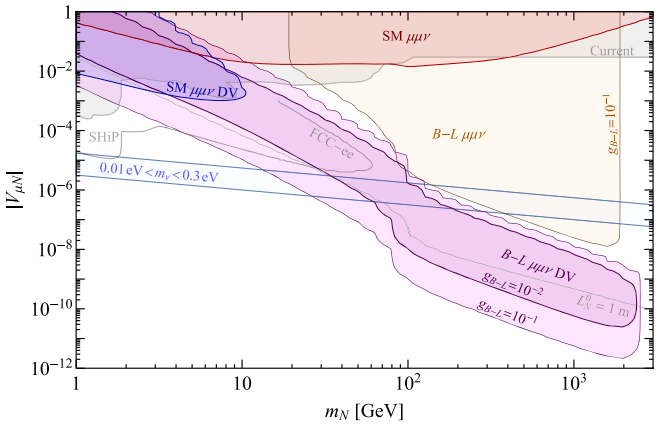

FIG. 8. Sensitivity of the FCC-hh with 30 ab^{-1} integrated luminosity at 95% CL towards the heavy neutrino production and leptonic $N \to \mu^+\mu^-\nu$ channel considered: SM W production with prompt (SM $\mu\mu\nu$, red) and displaced (SM $\mu\mu\nu$ DV, blue) vertices; $B-L$ Z' production with prompt ($B-L$ $\mu\mu\nu$, orange) and displaced ($B-L$ $\mu\mu\nu$ DV, purple) vertices. The $U(1)_{B-L}$ parameters are fixed at $m_{Z'} = 5$ TeV and $g_{B-L} = 10^{-2}, 0.1$ as indicated, with prompt $B-L$ $\mu\mu\nu$ not being sensitive at $g_{B-L} = 10^{-2}$. The light blue band corresponds to the regime with light neutrino masses 0.01 eV $< m_\nu <$ 0.3 eV via the see-saw mechanism. The shaded region labeled "current" is excluded by existing searches for heavy neutrinos [76], whereas "SHiP" and "FCC-ee" indicate the projected future sensitivity at the proposed SHiP [40] and FCC-ee [77], respectively. The proper heavy neutrino decay length L_N^0 of 1 m is indicated by the corresponding curve.

Both neutrinos are assumed to decay via $\mu\mu\nu$ in case of prompt $B-L$ production and thus leading to a $4\mu + \not{E}_T$ final state. The production channels and decay modes are accordingly labeled, e.g., "SM $\mu\mu\nu$ DV" denotes the SM production mode with $\mu\mu\nu$ final state, in a displaced vertex. Current best limits as collated in [76], which includes a displaced search at ATLAS [73] (small bump around $m_N \lesssim 10$ GeV), and projected sensitivities from the proposed SHiP [40] and FCC-ee [77] are also shown for comparison.

We start with analyzing the SM production channels in displaced (blue shaded region) and prompt (red shaded region) signatures. The striking feature for this production channel is the limited FCC-hh sensitivity. As shown in Sec. V C, this is because the p_T of the muons in the final state does not benefit from the larger collision energy. Instead, the stringent p_T requirements [$p_T(\mu) > 28$ GeV at the LHC [78] compared to $p_T(\mu) > 150$ GeV at the FCC-hh] limit the reach despite the increased cross section. Therefore, although the production cross section of N from this process can reach $\mathcal{O}(100)$ fb for active-sterile

[3]The two RH neutrinos can also decay leptonically and semileptonically, respectively, yielding a $3\mu + 2j + \not{E}_T$ final state. The main background comes from ZWW decays similarly, and its cross section is between the $4\mu + \text{MET}$ and $2\mu + 4j$ final states. We however do not consider this channel in this work as it should not give better sensitivity.

mixing $|V_{\mu N}| \sim 10^{-2}$, the FCC-hh fails to probe a significant parameter space as muons in the final states do not have sufficient p_T to pass the cuts.

Therefore, we obtain a sensitivity $|V_{\mu N}| \gtrsim 10^{-2}$ for the prompt final states of heavy neutrinos from the SM production at the FCC-hh, comparable to the reach of the LHC [4,11,79], as indicated by the "current" region. Although the cross section drops sharply as the W becomes off shell when $m_N > m_W$, p_T cuts become more efficient and the resulting sensitivity changes smoothly. The requirement of two same sign leptons helps with background control and in general leads to a sensitivity up to one order of magnitude stronger as compared to the opposite-sign signature. We therefore only show the sensitivity for the same-sign signature. For the displaced final states, as we look for heavy neutrinos with longer lifetime situated at lower $|V_{\mu N}|$, the gain due to negligible background is however canceled out by the reduced cross section, therefore the sensitivity to $|V_{\mu N}|$ becomes stronger by an order of magnitude only leading to $|V_{\mu N}| \gtrsim 10^{-3}$. The sensitivity vanishes for $m_N \gtrsim 10$ GeV, as the displaced final states requires $|V_{\mu N}| \sim 10^{-4}$, making the cross section insufficient to get any sensitivity in such a parameter space. Comparing to the projected limits from SHiP and FCC-hh, the FCC-hh is not competitive at lower m_N, but can have an advantage at greater m_N due to its larger collision energy.

The $B-L$ heavy neutrino production complements the SM channel. In the prompt $\mu\mu\nu$ final state, for $g_{B-L} = 10^{-1}$, the sensitivity extends up to $m_N = 2$ TeV and active-sterile mixing strengths $|V_{\mu N}|$ down to regimes where the heavy neutrino becomes long lived. Because both the neutrino production and decay branching ratios are independent of $|V_{\mu N}|$ (N does not decay to other flavors), only this promptness requirement limits the $|V_{\mu N}|$ reach. For the smaller value $g_{B-L} = 10^{-2}$, no sensitivity is obtained. For the displaced final state, the sensitivity in $V_{\mu N}$ follows heavy neutrino decay lengths between 1 mm $\lesssim L \lesssim$ 10 m, extending the $|V_{\mu N}|$ reach by about three orders of magnitude. The break at $m_N \approx 100$ GeV arises due to the change from off shell to on shell decays. It is worth noting that combining prompt and displaced final states, the seesaw mechanism responsible for generating light neutrino masses can be tested for 20 GeV $\lesssim m_N \lesssim m_{Z'}/2$, but displaced searches are also sensitive for $g_{B-L} = 10^{-2}$ assuming them being free of background.

The corresponding sensitivity arising from prompt and displaced μjj final states is shown in Fig. 9. In the prompt $B-L$ channel, both heavy neutrinos are assumed to decay as $N \to \mu jj$ thus leading to a $2\mu + 4j$ final state. We show the prompt final state sensitivity again only for the opposite-sign channel. The most important feature is the higher sensitivity as compared to $\mu\mu\nu$ final states in both displaced and prompt signatures because of the larger branching ratio of the semileptonic decay. For the SM

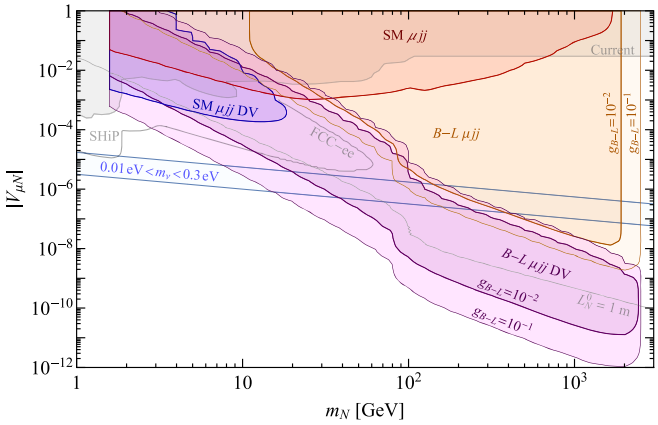

FIG. 9. As Fig. 8, but for the semileptonic final state μjj.

μjj prompt final state, it is now possible to reach $|V_{\mu N}| \approx 10^{-3}$ for $m_N \approx 30$ GeV. Similar to the SM mediated case, an increased sensitivity in both prompt and displaced final states can be found for $B-L$ heavy neutrino production as well. Otherwise, the overall sensitivity is similar to that of the fully leptonic mode but the prompt $B-L$ μjj case is also sensitive for $g_{B-L} = 10^{-2}$ up to masses of $m_N \lesssim 2$ TeV.

We have so far assumed $\epsilon_{\text{recon}} = 100\%$ to detect and reconstruct the displaced objects in the detector. This is clearly an idealized assumption. In a realistic scenario, the efficiencies will be highest near the primary vertex and will degrade towards outer parts of the detector (see, e.g., the discussion in [73,80]). To illustrate the impact of less than perfect efficiencies, we show in Fig. 10 the sensitivity of the $B-L$ μjj displaced final state as in Fig. 9 for an efficiency dependent on the lab frame decay length L_N of the heavy neutrino,

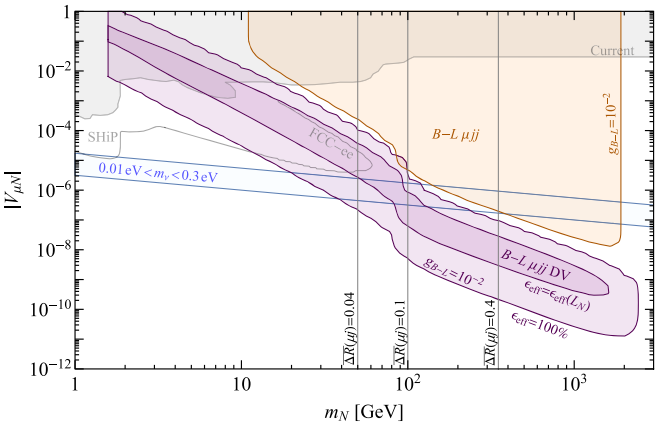

FIG. 10. As Fig. 9 but showing the displaced $B-L$ μjj sensitivity for both perfect ($\epsilon_{\text{eff}} = 100\%$) and reduced $\epsilon_{\text{eff}}(L_N)$ detection efficiency as described in the text. In addition, the vertical lines denote contours of the average $\overline{\Delta R}(\mu j) = 0.04$, 0.1, 0.4 between the muon and closest jet.

$$\epsilon_{\text{eff}}(L_N) = 0.002 \ln^2\left(\frac{L_N}{L_0}\right) \ln^2\left(\frac{L_N}{L_1}\right), \qquad (6.1)$$

for $L_0 < L_N < L_1$, and $\epsilon_{\text{eff}} = 0$ otherwise. Here, $L_0 = 0.025$ m and $L_1 = 5$ m are the boundaries of the inner tracker of the FCC-hh as shown in Fig. 1. Hence, we only consider the inner tracker in detecting displaced objects. The efficiency in Eq. (6.1) peaks at $\epsilon_{\text{eff}}(L_N) \approx 10\%$ for $L_N \approx 0.5$ m; i.e., we use a reduction of the order of that used in LHC analyses [73,80]. Such an order of magnitude reduction obviously worsens the FCC-hh reach but does not do so severely. As expected, the sensitivity is especially reduced in comparison with the $\epsilon_{\text{eff}} = 100\%$ case for smaller active-sterile mixing $|V_{\mu N}|$ as this corresponds to longer decay lengths.

As shown in Fig. 7, the muons and jets in the final states tend to be very collimated, and we also illustrate the average $\overline{\Delta R}(\mu j)$ between the muon and closest jet in Fig. 10. For $\overline{\Delta R}(\mu j) \lesssim 0.4$, i.e., $m_N \lesssim 300$ GeV, different analysis strategies are beneficial due to the collimated muons and jets. This, in principle, applies to both the prompt and displaced $B-L$ μjj signatures shown in Fig. 10. In the latter case, displaced fat jets can be considered which preserves sensitivity to small masses $m_N \gtrsim 10$ GeV [81]. For the prompt signature, the interesting region with $m_N \gtrsim 100$ GeV and $|V_{\mu N}| \approx 10^{-7} - 10^{-6}$, motivated by the light neutrino masses, corresponds to fairly large $\overline{\Delta R}(\mu j) \gtrsim 0.1$.

VII. CONCLUSION

The absence of an explanation of neutrino masses within the SM demands new physics. Experimental confirmation for such a mechanism will have a profound impact on understanding the fundamental laws of nature and will help build the next standard model. One such scenario is the seesaw mechanism in which heavy right-handed neutrinos are predicted. These can be produced at the LHC via Drell-Yan processes mediated by a SM W or a Z boson. The reach of colliders such as LHC or FCC is however limited as the heavy neutrino production is suppressed by the active-sterile mixing that is expected to be small to generate the correct light neutrino masses. This observation necessitates exploring nonminimal heavy neutrino production as a means to probe neutrino mass generation.

We have here determined the sensitivity of the FCC-hh towards heavy neutrino production within the $B-L$ model, which is equipped with an additional $B-L$ gauge boson Z'. Using this gauge boson as a portal of heavy neutrino production, we explored the process $pp \to Z' \to NN$ and we have contrasted the resulting sensitivity against the assured but suppressed SM production channel $pp \to W \to lN$. We have concentrated on muon flavor focusing on two different neutrino decay modes, $N \to \mu\mu\nu$ and $N \to \mu jj$. The FCC-hh with 30 ab^{-1} luminosity and 100 TeV center-of-mass energy can probe $B-L$ Z' gauge bosons with masses of the order 50 TeV. We use $m_{Z'} = 5$ TeV as benchmark with comparatively low values of the associated gauge coupling, namely $g_{B-L} = 10^{-2}$ and 0.1. With such a $U(1)_{B-L}$ portal, the FCC-hh will be able to probe regions relevant for neutrino mass generation in the $\mu\mu\nu$ and the μjj final state. Both prompt and displaced signals are relevant to cover a range of heavy neutrino mass 20 GeV $\lesssim m_N \lesssim 2$ TeV with active-sterile mixing strength $|V_{\mu N}| \approx 10^{-7} - 10^{-5}$ motivated by light neutrino masses, $m_\nu \sim |V_{\mu N}|^2 m_N \sim 0.1$ eV. In the given scenario considered, active-sterile mixing strengths as low as $V_{\mu N} \approx 10^{-12}$ can be probed. Such searches for displaced heavy neutrinos have smaller background and thus may even be the first direct signal of an exotic Z' resonance, potentially shedding light on the R_K anomaly [82].

The neutrino production processes mediated by the SM W and Z, while assured and independent of the $U(1)_{B-L}$ extension, are suppressed by this active-sterile mixing. Only dedicated facilities with high fluxes and the potential to probe long lived particles such as SHiP and FCC-ee have the ability to probe the required small active-sterile mixing strength but only for limited ranges of neutrino masses, namely $m_N \approx 1$–2 GeV and $m_N \approx 50$ GeV, respectively. In the same channel, the FCC-hh will only be able to probe active-sterile mixing strengths $|V_{\mu N}| \approx 10^{-3} - 10^{-4}$, to high for a successful generic seesaw mechanism. This sensitivity is also comparable to the HL-LHC; the gain in terms of luminosity and cross section are compensated by the harder p_T requirements.

While the mechanism of neutrino mass generation may be adapted to incorporate heavy neutrinos with large active-sterile mixing, such as in inverse seesaw scenarios, the vanilla seesaw remains an attractive and suggestive proposition. The corresponding Yukawa couplings between the left- and right-handed neutrinos may be small, $y_\nu \approx 10^{-6}$ for m_N around the electroweak scale, but this is of the order of the Yukawa coupling of the electron. The minimal $B-L$ model has the appeal of incorporating the origin of light neutrino masses by breaking lepton number spontaneously. This is still possible near the electroweak scale and, as we have shown, it can lead to striking prompt and displaced signatures. Heavy neutrino production via a Z' mediator has the potential to probe regions of parameter space relevant for neutrino mass generation in multiple final states. A refinement of our analysis with a full detector simulation should be able to demonstrate the reach more accurately, however, our first exploration demonstrates the potential of the FCC to target heavy neutrinos and the origin of light neutrinos.

ACKNOWLEDGMENTS

W. L. is supported by the 2021 Jiangsu Shuangchuang (Mass Innovation and Entrepreneurship) Talent Program (JSSCBS20210213). S. K. is supported by Elise-Richter Grant Project No. V592-N27 and F. F. D. by a UK STFC consolidated grant (Reference ST/P00072X/1). The authors would like to thank F. Blekman, S. Pagan Griso, and O. Fischer for several useful discussions.

[1] A. Davidson, $B - L$ as the fourth color within an $SU(2)_L \times U(1)_R \times U(1)$ model, Phys. Rev. D **20**, 776 (1979).
[2] R. N. Mohapatra and R. Marshak, Local B-L Symmetry of Electroweak Interactions, Majorana Neutrinos and Neutron Oscillations, Phys. Rev. Lett. **44**, 1316 (1980).
[3] S. Chatrchyan *et al.* (CMS Collaboration), Search for heavy Majorana neutrinos in $\mu^{\pm}\mu^{\pm} +$ jets and $e^{\pm}e^{\pm} +$ jets events in pp collisions at $\sqrt{s} = 7$ TeV, Phys. Lett. B **717**, 109 (2012).
[4] R. Aaij *et al.* (LHCb Collaboration), Search for Majorana Neutrinos in $B^- \to \pi^+\mu^-\mu^-$ decays, Phys. Rev. Lett. **112**, 131802 (2014).
[5] G. Aad *et al.* (ATLAS Collaboration), Search for heavy Majorana neutrinos with the ATLAS detector in pp collisions at $\sqrt{s} = 8$ TeV, J. High Energy Phys. 07 (2015) 162.
[6] V. Khachatryan *et al.* (CMS Collaboration), Search for heavy Majorana neutrinos in $\mu^{\pm}\mu^{\pm} +$ jets events in proton-proton collisions at $\sqrt{s} = 8$ TeV, Phys. Lett. B **748**, 144 (2015).
[7] V. Khachatryan *et al.* (CMS Collaboration), Search for heavy Majorana neutrinos in $e^{\pm}e^{\pm} +$ jets and $e^{\pm}\mu^{\pm} +$ jets events in proton-proton collisions at $\sqrt{s} = 8$ TeV, J. High Energy Phys. 04 (2016) 169.
[8] E. Cortina Gil *et al.* (NA62 Collaboration), Search for heavy neutral lepton production in K^+ decays, Phys. Lett. B **778**, 137 (2018).
[9] P. Mermod (SHiP Collaboration), Prospects of the SHiP and NA62 experiments at CERN for hidden sector searches, Proc. Sci. NuFact2017 (**2017**) 139 [arXiv:1712.01768].
[10] A. Izmaylov and S. Suvorov, Search for heavy neutrinos in the ND280 near detector of the T2K experiment, Phys. Part. Nucl. **48**, 984 (2017).
[11] A. M. Sirunyan *et al.* (CMS Collaboration), Search for Heavy Neutral Leptons in Events with Three Charged Leptons in Proton-Proton Collisions at $\sqrt{s} = 13$ TeV, Phys. Rev. Lett. **120**, 221801 (2018).
[12] J. C. Helo, S. Kovalenko, and I. Schmidt, Sterile neutrinos in lepton number and lepton flavor violating decays, Nucl. Phys. **B853**, 80 (2011).
[13] D. Liventsev *et al.* (Belle Collaboration), Search for heavy neutrinos at Belle, Phys. Rev. D **87**, 071102 (2013).
[14] A. Abada, A. Teixeira, A. Vicente, and C. Weiland, Sterile neutrinos in leptonic and semileptonic decays, J. High Energy Phys. 02 (2014) 091.
[15] J. C. Helo, M. Hirsch, and S. Kovalenko, Heavy neutrino searches at the LHC with displaced vertices, Phys. Rev. D **89**, 073005 (2014).
[16] L. Canetti, M. Drewes, and B. Garbrecht, Probing leptogenesis with GeV-scale sterile neutrinos at LHCb and Belle II, Phys. Rev. D **90**, 125005 (2014).
[17] A. M. Gago, P. Hernández, J. Jones-Pérez, M. Losada, and A. Moreno Briceño, Probing the Type I seesaw mechanism with displaced vertices at the LHC, Eur. Phys. J. C **75**, 470 (2015).
[18] A. Das and N. Okada, Improved bounds on the heavy neutrino productions at the LHC, Phys. Rev. D **93**, 033003 (2016).
[19] S. Banerjee, P. S. B. Dev, A. Ibarra, T. Mandal, and M. Mitra, Prospects of heavy neutrino searches at future lepton colliders, Phys. Rev. D **92**, 075002 (2015).
[20] E. Izaguirre and B. Shuve, Multilepton and lepton jet probes of sub-weak-scale right-handed neutrinos, Phys. Rev. D **91**, 093010 (2015).
[21] E. Arganda, M. Herrero, X. Marcano, and C. Weiland, Exotic $\mu\tau$jj events from heavy ISS neutrinos at the LHC, Phys. Lett. B **752**, 46 (2016).
[22] S. Antusch and O. Fischer, Testing sterile neutrino extensions of the Standard Model at future lepton colliders, J. High Energy Phys. 05 (2015) 053.
[23] C. Degrande, O. Mattelaer, R. Ruiz, and J. Turner, Fully-automated precision predictions for heavy neutrino production mechanisms at hadron colliders, Phys. Rev. D **94**, 053002 (2016).
[24] S. Antusch, E. Cazzato, M. Drewes, O. Fischer, B. Garbrecht, D. Gueter, and J. Klarić, Probing leptogenesis at future colliders, J. High Energy Phys. 09 (2018) 124.
[25] R. Ruiz, M. Spannowsky, and P. Waite, Heavy neutrinos from gluon fusion, Phys. Rev. D **96**, 055042 (2017).
[26] S. Antusch, E. Cazzato, and O. Fischer, Sterile neutrino searches via displaced vertices at LHCb, Phys. Lett. B **774**, 114 (2017).
[27] S. Dube, D. Gadkari, and A. M. Thalapillil, Lepton-jets and low-mass sterile neutrinos at hadron colliders, Phys. Rev. D **96**, 055031 (2017).
[28] Y. Cai, T. Han, T. Li, and R. Ruiz, Lepton number violation: Seesaw models and their collider tests, Front. Phys. **6**, 40 (2018).
[29] F. F. Deppisch, W. Liu, and M. Mitra, Long-lived heavy neutrinos from Higgs decays, J. High Energy Phys. 08 (2018) 181.
[30] A. Abada, N. Bernal, M. Losada, and X. Marcano, Inclusive displaced vertex searches for heavy neutral leptons at the LHC, J. High Energy Phys. 01 (2019) 093.
[31] G. Cottin, J. C. Helo, and M. Hirsch, Displaced vertices as probes of sterile neutrino mixing at the LHC, Phys. Rev. D **98**, 035012 (2018).

[32] M. Drewes, J. Hajer, J. Klaric, and G. Lanfranchi, NA62 sensitivity to heavy neutral leptons in the low scale seesaw model, J. High Energy Phys. 07 (2018) 105.
[33] C. O. Dib, C. Kim, N. A. Neill, and X.-B. Yuan, Search for sterile neutrinos decaying into pions at the LHC, Phys. Rev. D **97**, 035022 (2018).
[34] I. Boiarska, K. Bondarenko, A. Boyarsky, S. Eijima, M. Ovchynnikov, O. Ruchayskiy *et al.*, Probing baryon asymmetry of the Universe at LHC and SHiP, arXiv:1902.04535.
[35] K. Cheung, Y.-L. Chung, H. Ishida, and C.-T. Lu, Sensitivity reach on heavy neutral leptons and τ-neutrino mixing $|U_{\tau N}|^2$ at the HL-LHC, Phys. Rev. D **102**, 075038 (2020).
[36] J. Jones-Pérez, J. Masias, and J. D. Ruiz-Álvarez, Search for long-lived heavy neutrinos at the LHC with a VBF trigger, Eur. Phys. J. C **80**, 642 (2020).
[37] J. Liu, Z. Liu, L.-T. Wang, and X.-P. Wang, Seeking for sterile neutrinos with displaced leptons at the LHC, J. High Energy Phys. 07 (2019) 159.
[38] M. Drewes and J. Hajer, Heavy Neutrinos in displaced vertex searches at the LHC and HL-LHC, J. High Energy Phys. 02 (2020) 070.
[39] S. Alekhin *et al.*, A facility to search for hidden particles at the CERN SPS: The SHiP physics case, Rep. Prog. Phys. **79**, 124201 (2016).
[40] C. Ahdida *et al.* (SHiP Collaboration), Sensitivity of the SHiP experiment to heavy neutral leptons, J. High Energy Phys. 04 (2019) 077.
[41] A. Das, S. Jana, S. Mandal, and S. Nandi, Probing right handed neutrinos at the LHeC and lepton colliders using fat jet signatures, Phys. Rev. D **99**, 055030 (2019).
[42] S. Antusch, E. Cazzato, and O. Fischer, Sterile neutrino searches at future e^-e^+, pp, and e^-p colliders, Int. J. Mod. Phys. A **32**, 1750078 (2017).
[43] S. Pascoli, R. Ruiz, and C. Weiland, Heavy neutrinos with dynamic jet vetoes: multilepton searches at $\sqrt{s} = 14$, 27, and 100 TeV, J. High Energy Phys. 06 (2019) 049.
[44] C.-W. Chiang, G. Cottin, A. Das, and S. Mandal, Displaced heavy neutrinos from Z' decays at the LHC, J. High Energy Phys. 12 (2019) 070.
[45] F. F. Deppisch, N. Desai, and J. W. F. Valle, Is charged lepton flavor violation a high energy phenomenon?, Phys. Rev. D **89**, 051302 (2014).
[46] B. Batell, M. Pospelov, and B. Shuve, Shedding light on neutrino masses with dark forces, J. High Energy Phys. 08 (2016) 052.
[47] F. Deppisch, S. Kulkarni, and W. Liu, Heavy neutrino production via Z' at the lifetime frontier, Phys. Rev. D **100**, 035005 (2019).
[48] B. Bhattacherjee, S. Matsumoto, and R. Sengupta, Long-lived light mediators from Higgs boson decay at HL-LHC, FCC-hh and a proposal of dedicated LLP detectors for FCC-hh, arXiv:2111.02437.
[49] E. Accomando, L. Delle Rose, S. Moretti, E. Olaiya, and C. H. Shepherd-Themistocleous, Extra Higgs boson and Z' as portals to signatures of heavy neutrinos at the LHC, J. High Energy Phys. 02 (2018) 109.
[50] A. Das, P. B. Dev, and N. Okada, Long-lived TeV-scale right-handed neutrino production at the LHC in gauged $U(1)_X$ model, Phys. Lett. B **799**, 135052 (2019).
[51] K. Cheung, K. Wang, and Z. S. Wang, Time-delayed electrons from neutral currents at the LHC, J. High Energy Phys. 09 (2021) 026.
[52] P. Fileviez Pérez and A. D. Plascencia, Probing the nature of neutrinos with a new force, Phys. Rev. D **102**, 015010 (2020).
[53] E. Accomando, L. Delle Rose, S. Moretti, E. Olaiya, and C. H. Shepherd-Themistocleous, Novel SM-like Higgs decay into displaced heavy neutrino pairs in U(1)' models, J. High Energy Phys. 04 (2017) 081.
[54] C. Han, T. Li, and C.-Y. Yao, Searching for heavy neutrino in terms of tau lepton at future hadron collider, Phys. Rev. D **104**, 015036 (2021).
[55] F. F. Deppisch and A. Pilaftsis, Lepton flavour violation and theta(13) in minimal resonant leptogenesis, Phys. Rev. D **83**, 076007 (2011).
[56] A. Atre, T. Han, S. Pascoli, and B. Zhang, The search for heavy Majorana neutrinos, J. High Energy Phys. 05 (2009) 030.
[57] A. Abada *et al.* (FCC Collaboration), FCC-hh: The hadron collider: Future circular collider conceptual design report volume 3, Eur. Phys. J. Spec. Top. **228**, 755 (2019).
[58] CMS Collaboration, Search for a narrow resonance in high-mass dilepton final states in proton-proton collisions using 140 fb^{-1} of data at $\sqrt{s} = 13$ TeV, CERN Report No. CMS-PAS-EXO-19-019, https://inspirehep.net/literature/1747703.
[59] A. M. Sirunyan *et al.* (CMS Collaboration), Search for resonant and nonresonant new phenomena in high-mass dilepton final states at $\sqrt{s} = 13$ TeV, J. High Energy Phys. 07 (2021) 208.
[60] C. Helsens, D. Jamin, M. L. Mangano, T. G. Rizzo, and M. Selvaggi, Heavy resonances at energy-frontier hadron colliders, Eur. Phys. J. C **79**, 569 (2019).
[61] F. Blekman (private communication).
[62] C. Degrande, C. Duhr, B. Fuks, D. Grellscheid, O. Mattelaer, and T. Reiter, UFO—The universal FeynRules output, Comput. Phys. Commun. **183**, 1201 (2012).
[63] J. Alwall, R. Frederix, S. Frixione, V. Hirschi, F. Maltoni, O. Mattelaer, H.-S. Shao, T. Stelzer, P. Torrielli, and M. Zaro, The automated computation of tree-level and next-to-leading order differential cross sections, and their matching to parton shower simulations, J. High Energy Phys. 07 (2014) 079.
[64] A. Alloul, N. D. Christensen, C. Degrande, C. Duhr, and B. Fuks, FeynRules 2.0—A complete toolbox for tree-level phenomenology, Comput. Phys. Commun. **185**, 2250 (2014).
[65] N. D. Christensen and C. Duhr, FeynRules—Feynman rules made easy, Comput. Phys. Commun. **180**, 1614 (2009).
[66] Feynrulesdatabase, https://feynrules.irmp.ucl.ac.be/wiki/B-L-SM.
[67] T. Sjöstrand, S. Ask, J. R. Christiansen, R. Corke, N. Desai, P. Ilten, S. Mrenna, S. Prestel, C. O. Rasmussen, and P. Z. Skands, An introduction to PYTHIA 8.2, Comput. Phys. Commun. **191**, 159 (2015).
[68] M. Cacciari, G. P. Salam, and G. Soyez, FastJet user manual, Eur. Phys. J. C **72**, 1896 (2012).
[69] F. F. Deppisch, S. Kulkarni, and W. Liu, Searching for a light Z' through Higgs production at the LHC, Phys. Rev. D **100**, 115023 (2019).

[70] S. Amrith, J. M. Butterworth, F. F. Deppisch, W. Liu, A. Varma, and D. Yallup, LHC constraints on a $B-L$ gauge model using contur, J. High Energy Phys. 05 (2019) 154.
[71] G. Aad *et al.* (ATLAS Collaboration), Search for high-mass dilepton resonances using 139 fb^{-1} of pp collision data collected at $\sqrt{s}=13$ TeV with the ATLAS detector, Phys. Lett. B **796**, 68 (2019).
[72] M. Aaboud *et al.* (ATLAS Collaboration), Electron reconstruction and identification in the ATLAS experiment using the 2015 and 2016 LHC proton-proton collision data at $\sqrt{s}=13$ TeV, Eur. Phys. J. C **79**, 639 (2019).
[73] G. Aad *et al.* (ATLAS Collaboration), Search for heavy neutral leptons in decays of W bosons produced in 13 TeV pp collisions using prompt and displaced signatures with the ATLAS detector, J. High Energy Phys. 10 (2019) 265.
[74] R. Aaij *et al.* (LHCb Collaboration), Search for long-lived particles decaying to $e^{\pm}\mu^{\mp}\nu$, Eur. Phys. J. C **81**, 261 (2021).
[75] A. Tumasyan *et al.* (CMS Collaboration), Search for long-lived heavy neutral leptons with displaced vertices in proton-proton collisions at $\sqrt{s}=13$ TeV, arXiv:2201.05578.
[76] P. D. Bolton, F. F. Deppisch, and P. S. Bhupal Dev, Neutrinoless double beta decay versus other probes of heavy sterile neutrinos, J. High Energy Phys. 03 (2020) 170.
[77] A. Blondel, E. Graverini, N. Serra, and M. Shaposhnikov (FCC-ee study Team), Search for Heavy Right Handed Neutrinos at the FCC-ee, Nucl. Part. Phys. Proc. **273–275**, 1883 (2016).
[78] M. Aaboud *et al.* (ATLAS Collaboration), Search for new high-mass phenomena in the dilepton final state using 36 fb^{-1} of proton-proton collision data at $\sqrt{s}=13$ TeV with the ATLAS detector, J. High Energy Phys. 10 (2017) 182.
[79] G. Aad *et al.* (ATLAS Collaboration), Search for heavy neutral leptons in decays of W bosons produced in 13 TeV pp collisions using prompt and displaced signatures with the ATLAS detector, J. High Energy Phys. 10 (2019) 265.
[80] ATLAS Collaboration, Performance of vertex reconstruction algorithms for detection of new long-lived particle decays within the ATLAS inner detector, CERN Technical Report No. ATL-PHYS-PUB-2019-013, https://inspirehep.net/literature/1795240.
[81] R. Padhan, M. Mitra, S. Kulkarni, and F. F. Deppisch, Displaced fat-jets and tracks to probe boosted right-handed neutrinos in the $U(1)_{B-L}$ model, arXiv:2203.06114.
[82] A. Falkowski, S. F. King, E. Perdomo, and M. Pierre, Flavourful Z' portal for vector-like neutrino Dark Matter and $R_{K^{(*)}}$, J. High Energy Phys. 08 (2018) 061.